Biomimetic organization: Octapeptide self-assembly into nanotubes of viral capsid-like dimension

Céline Valéry[†], Maïté Paternostre[†§], Bruno Robert[‡], Thaddée Gulik-Krzywicki[¶], Theyencheri Narayanan[∥], Jean-Claude Dedieu[¶], Gérard Keller[†], Maria-Luisa Torres[††], Roland Cherif-Cheikh[††], Pilar Calvo[††], and Franck Artzner[†§‡‡]

[†]Unité Mixte de Recherche 8612, Centre National de la Recherche Scientifique, Faculté de Pharmacie, 5 Rue J.B. Clément, 92296 Châtenay-Malabry Cedex, France; [‡]Service de Biophysique des Fonctions Membranaires, Département de Biologie Joliot Curie, Unité de Recherche Associée 2096, Centre National de la Recherche Scientifique, Commissariat à l'Energie Atomique–Saclay, 91191 Gif-sur-Yvette, France; [¶]Centre de Génétique Moléculaire, Centre National de la Recherche Scientifique, 91198 Gif-sur-Yvette, France; [∥]European Synchrotron Radiation Facility, BP 220, 38403 Grenoble Cedex, France; and [††]Ipsen Pharma S.A., Ctra. Laureà Miró 395, 08980-Sant Feliu de Llobregat, Barcelona, Spain

The controlled self-assembly of complex molecules into well defined hierarchical structures is a promising route for fabricating nanostructures. These nanoscale structures can be realized by naturally occurring proteins such as tobacco mosaic virus, capsid proteins, tubulin, actin, etc. Here, we report a simple alternative method based on self-assembling nanotubes formed by a synthetic therapeutic octapeptide, Lanreotide in water. We used a multidisciplinary approach involving optical and electron microscopies, vibrational spectroscopies, and small and wide angle x-ray scattering to elucidate the hierarchy of structures exhibited by this system. The results revealed the hexagonal packing of nanotubes, and high degree of monodispersity in the tube diameter (244 Å) and wall thickness (≈18 Å). Moreover, the diameter is tunable by suitable modifications in the molecular structure. The self-assembly of the nanotubes occurs through the association of β-sheets driven by amphiphilicity and a systematic aromatic/aliphatic side chain segregation. This original and simple system is a unique example for the study of complex self-assembling processes generated by de novo molecules or amyloid peptides.

The ability of simple molecules to spontaneously organize into well defined nanostructures is of fundamental importance and has wide ranging applications in biotechnology and materials sciences (1). In fact, characteristic lengths <100 nm are not easily accessible at present by lithographic techniques, but can be realized with biological self-assemblies such as tobacco mosaic virus, capsid proteins (2), tubulin (3), or actin (4, 5). These proteins under appropriate conditions possess the unique capability to form long filaments with a well defined diameter. However, the fabrication cost often restricts their potential interest in practical applications. Therefore, a simple alternative route has been emerged based on de novo molecules that self-organize in a programmed way (6–11). The design of such biomimetic systems requires the understanding of the relationship between the molecular structure and the self-assembly process of the nanostructures. This inspiration from natural fibers is difficult to implement when the building blocks themselves are complex, as in the case of proteins. Up to now, no simple synthetic molecule was able to self-assemble into hollow nanotubes with well defined characteristic length in the range of 20–30 nm.

Lanreotide is an octapeptide synthesized as a growth hormone inhibitor. Lanreotide forms hydrogels (Autogel), which are already used in acromegaly treatment as s.c. long-acting implants (12). Here we report the molecular and supramolecular organization of self-assembling nanotubes formed by Lanreotide in water (10% wt/wt, acetate salt). We chose a multidisciplinary approach, by combining polarized light microscopy, electron microscopy, vibrational spectroscopies, small and wide angle x-ray scattering (SAXS and WAXS, respectively) to elucidate the hierarchical structures formed by this system. The nanotubes are remarkably monodisperse, with a diameter of 244 Å and a wall thickness of ≈18 Å. The study of a Lanreotide derivative

indicates the possibility to control the diameter of these tubes from the molecular structure. The self-assembly of these nanotubes occurs through the association of β-sheets driven by amphiphilicity and a systematic aromatic/aliphatic side chain segregation. This original and simple system is a unique example of molecules able to self-organize into well defined nanostucture. The resolution of the structure at the molecular scale highlights the simplicity of the interactions involved in the self-assembly process, and could find implication for β-amyloid fibers or de novo self-assemblies.

Materials and Methods

Materials. Cyclic Lanreotide of sequence NH_2-(D)Naph-Cys-Tyr-(D)Trp-Lys-Val-Cys-Thr-$CONH_2$ (BIM 23014C) and its cyclic derivative of sequence NH_2-(D)Naph-Cys-Tyr-(D)Phe-Lys-Val-Cys-Thr-$CONH_2$ (BIM 23A462C) were obtained from Ipsen Pharma (Barcelona) as acetate salts (molecular masses of 1,095 and 1,060 Da, respectively, purity >98%). Mixtures were made by dissolving the peptides powders at 10–14% wt/wt in pure water. Glycerol (99.9%) was purchased from Sigma.

Optical Microscopy. Very thin preparations between glass slides were observed with a Nikon microscope equipped with two crossed polarizers. A color plate was used to analyze the deformation orientations.

Electron Microscopy. Electron microscopy observations were preceded by freeze-fracture and freeze-etching of samples containing 30% wt/wt dried glycerol as cryoprotectant. Small aliquots of the samples were placed on copper grids, frozen in liquid propane, and stored in liquid nitrogen. Freeze-fracture, freeze-etching, and replication were successively performed by using a Balzers 301 apparatus equipped with an electron gun for platinum shadowing. Replicates were examined by using a Philips 301 electron microscope.

SAXS. X-ray diffraction experiments were performed at the High Brilliance beam line (ID2), European Synchrotron Radiation Facility in Grenoble, France (13). The undulator x-ray beam (of wavelength 0.99 Å) was selected by a channel-cut Si(111) crystal, and focused by rhodium-coated toroidal mirror. The beam size defined by the collimating slits was 0.2 mm × 0.2 mm. The detector was an image intensified charge-coupled device camera, and the sample-to-detector distance varied between 150 and 650 cm.

X-Ray Fiber Diffraction and Analysis. The setup was the same as in SAXS, with a sample-detector distance of 90 cm. In addition, high-resolution x-ray patterns were collected with a 45×36-cm^2 image-plate detector at a distance of 65 cm. Theoretically, the fiber diffraction pattern (14) is horizontal layer lines localized in the reciprocal space at $q_z = lc^*$ and whose intensity $I_l(q_r)$ is

$$I_l(q_r) = |\langle F_l(q_r, \Psi, lc^*)\rangle|^2, \qquad [1]$$

where Ψ, q_r, and q_z are the angular, radial, and axial cylindrical coordinates of the reciprocal space, and with

$$F_l(q_r, \Psi, lc^*) = \sum_{n=-\infty}^{+\infty} F_{nl}(q_r)\exp[in\Psi] \qquad [2]$$

$$F_{nl}(q_r) = \exp\left(in\frac{\pi}{2}\right)\int_0^\infty \rho_{nl}(r)J_n(2\pi r)2\pi r\, dr, \qquad [3]$$

where J_n is the Bessel function of order n and

$$\rho_{nl}(r) = \frac{1}{2\pi}\int_0^{2\pi}\int_0^c \rho_M(r, \psi, z)\exp\left[-i\left(n\psi - \frac{2\pi lz}{c}\right)\right]dr\, d\psi, \qquad [4]$$

where $\rho_M(r, \psi, z)$ is the electron density of the tube function in cylindrical coordinate ψ, r, and z. In the case of a thin cylinder of radius r_0, the diffuse scattering is reduced to horizontal lines with intensity profiles $I(q_r.r_0)$. For peaks corresponding to $q = h.\mathbf{i}^* + k.\mathbf{j}^*$, with $\mathbf{i}^*$ and $\mathbf{j}^*$ the reciprocal vectors of the $(\mathbf{i}, \mathbf{j})$ lattice, the profile is a Bessel function of order $l = h.n + k.m$, i.e., $I(q_r.r_0) = [J_l(q_r.r_0)/q_r.r_0]^2$, and the vertical position is $q_z = h.\mathbf{i}_z^* + k.\mathbf{j}_z^*$.

Fourier-Transform Raman Spectroscopy. Spectra were recorded at 4 cm^{-1} resolution by using a Bruker IFS 66 interferometer coupled to a Bruker FRA 106 Raman module equipped with a continuous Nd:YAG laser providing excitation at 1,064 nm. All spectra were recorded at room temperature with backscattering geometry from concentrated samples held in standard aluminum cups. The spectra obtained resulted from 5,000 coadded interferograms.

Fourier-Transform Infrared Spectroscopy. Attenuated total reflectance (ATR) Fourier transform infrared spectra were measured at a 2-cm^{-1} resolution with a Bruker IFS 66 spectrophotometer equipped with a 45° N ZnSe ATR attachment. The spectra obtained resulted from the average of 50 scans and were corrected for the linear dependence on the wavelength of the absorption measured by ATR. The water signal was removed by subtraction of pure water spectrum. Analysis of the conformations of the peptides was performed by deconvolution of the absorption spectra as a sum of Gaussian components.

Results

Nanotube Morphology and Organization. Lanreotide acetate and its derivative spontaneously form gels in water at 10% (wt/wt) concentration. Optical textures observed between crossed polarizers (Fig. 1) are developable surfaces, which are compatible with a columnar hexagonal liquid-crystal phase. Electron micrographs of freeze-etching replicates show tightly packed long and thin nanotubes (Fig. 2 *a* and *b*). In the case of Lanreotide, SAXS experiments reveal that these nanotubes have a 2D hexagonal packing with a lattice parameter (a_{hex}) of 365 Å, a monodisperse diameter (ϕ) of 244 Å and a wall thickness (e) of ≈ 18 Å (Fig. 2 *c* and *d*). Moreover, the absence of order along the
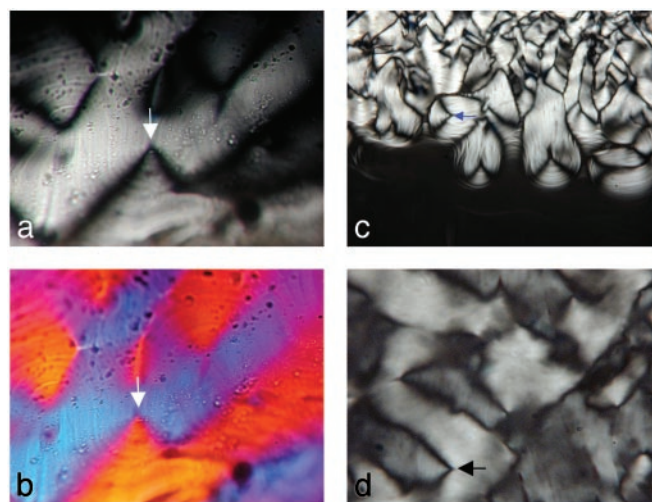

Fig. 1. Optical textures of hexagonal columnar phases of Lanreotide (*a* and *b*) and its derivative (*c* and *d*) observed between cross-polarizers (±45°) through thin preparations (magnification, ×2,500). A color plate is added in *b*. (*c*) Texture growing from isotropic liquid (magnification, ×1,250). The observed fan-shape textures are characteristic deformations of parallel planes in developable surfaces (arrows). These deformations are compatible with hexagonal columnar liquid-crystal phases (or lamellar phases).

direction of the tubes axis demonstrates that the nanotubes freely slide in a hexagonal liquid crystalline phase (15, 16).

Lanreotide Conformation. FT-Raman spectroscopy shows the presence of a disulfide bridge in the Lanreotide structure, with a *gauche–gauche–gauche* conformation as evidenced by the presence of the characteristic 506-cm^{-1} vibration (Fig. 3*a*) (17). The amide I vibrations observed by Fourier transform infrared spectroscopy indicate that 35% of the hydrogen bonds implying backbone carbonyl groups are involved in antiparallel β-sheet, 15% in turn and 50% in random conformations (Fig. 3*b*) (18). These data strongly support a planar β-hairpin conformation for the peptide backbone with a turn located at the D-tryptophan residue, which is stabilized by the disulfide bridge and intramolecular hydrogen bonds. This conformation enhances the amphiphilic nature of the peptide by exposing the hydrophilic disulfide bridge on one face of the β-hairpin, whereas the hydrophobic residues are exposed on the other face. Furthermore, the aromatic residues are segregated from the aliphatic ones, each being located on one β-strand. Given the β-hairpin conformation, three couples of hydrogen bond donors/acceptors are in the right orientation to form a β-sheet fiber.

Fiber Diffraction. The organization within the nanotube wall is crystalline as shown by an exceptionally well aligned WAXS pattern (mosaicity <0.5°) acquired with the Lanreotide derivative (Fig. 4*a*). This diffraction pattern can be unambiguously interpreted in terms of a 2D curved crystal (further analysis reveals the formation of ripples along the $\mathbf{i}$ vector constituted by two filaments). The position of diffuse scattering maxima can be indexed by a 2D monoclinic lattice $\mathbf{i} = 20.7$ Å, $\mathbf{j} = 20.8$ Å, $\gamma = 117.2°$, with $\mathbf{j}$ at an angle of 48.3° with respect to the direction of the cylinder axis. The line shapes of the diffuse scattering can be simulated (Fig. 4 *b* and *c*) by Bessel functions corresponding to the Fourier transform of a 2D lattice (Fig. 4*d*). The molecular organization of both Lanreotide and its derivative are identical as indicated by the similarity of all of the cell parameters (Table 1). In both cases, the Patterson function of the nanotube walls, calculated from the main diffuse scattering, reveals a 20.8 Å alternation of low and high electron density along the $\mathbf{j}$ vector
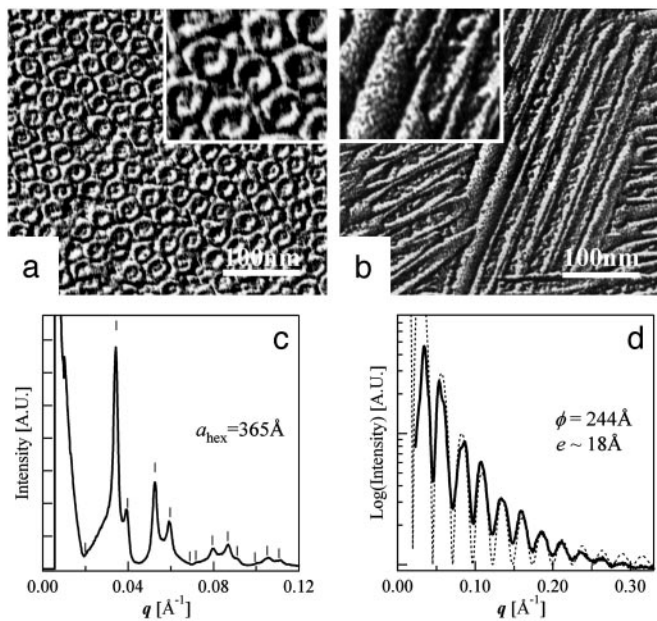
Fig. 2. Characterization of Lanreotide nanotubes. (*a* and *b*) Freeze-fracture electron micrographs of a 14% wt/wt Lanreotide acetate–water sample. The planes of fracture are perpendicular (*a*) and parallel (*b*) to the director of the tightly packed thin tubes. (*Insets*) A ×2 enlargement of the corresponding micrographs. (*c*) SAXS with sample–detector distance of 6 m. Superimposed lines indicate calculated values in the case of a 2D columnar hexagonal phase with a packing parameter a_{hex} of 365 Å, which corresponds to the distance between the centers of the nanotubes. (*d*) SAXS with a sample–detector distance of 1.5 m. The diffraction peaks are not resolved, but their envelope (form factor) is observed. The zeros are in agreement with a Bessel function $(J_0(q \cdot r_0)/q \cdot r_0)^2$ (dashed curve), which corresponds to the form factor of a monodisperse cylinder of radius $r_0 = 122$ Å. The wall thickness of the nanotubes, estimated from the position of the last oscillation, is ≈18 Å.

(Fig. 4*e*), i.e., a segregation between aromatic/aliphatic residues. A β-sheet stacking made by a unique peptide translation leads to a repeat distance of ≈9.4 Å (2 × 4.7 Å) and is not in agreement with the experimental one of 20.8 Å. Moreover, such a stacking would not create the aromatic/aliphatic alternation. On the contrary, β-sheet fibers built from an alternated
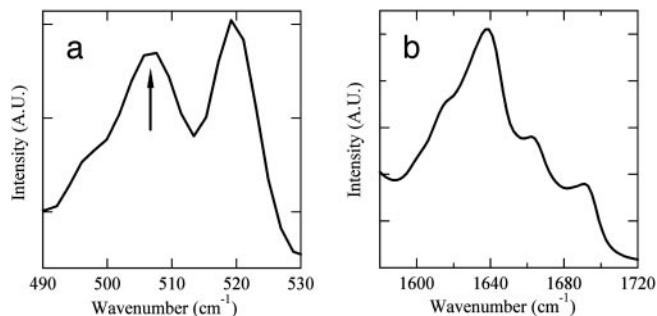

Fig. 3. Conformation of Lanreotide in the nanotubes determined by vibrational spectroscopies. (*a*) Fourier transform (FT)–Raman spectroscopy. The figure shows the frequency range of disulfide bond vibrations. The 506-cm^{-1} vibration (arrow) indicates a *gauche–gauche–gauche* disulfide bridge. The 519-cm^{-1} vibration is characteristic of the Naphthalene ring of the D-naphthylalanine residue. (*b*) Fourier transform infrared spectrum of the amide I region (vibrations of the carbonyl groups) after subtraction of the water contribution. The percentages of backbone carbonyls involved in hydrogen bonds in different conformations have been estimated after deconvolution, i.e., 35% of antiparallel β-sheet (1,618 and 1,689 cm^{-1}), 15% of turn (1,663 cm^{-1}), and 50% of random (1,639 cm^{-1}).
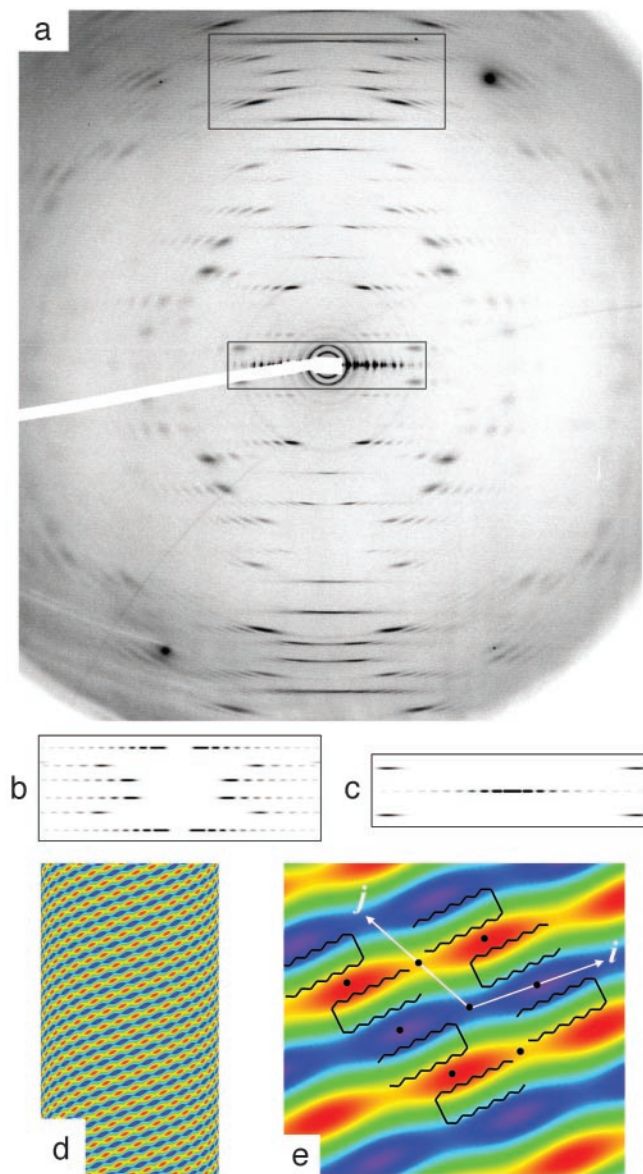

Fig. 4. Crystalline structure of the wall of Lanreotide nanotubes. (*a*) High-resolution fiber diffraction of the Lanreotide derivative at 10% wt/wt (acetate) in water. (*b* and *c*) Simulations of diffuse scattering at wide angles (WAXS) of selected zones (rectangles in *a*). (*d*) Two-dimensional Patterson function indicating the main electron density variations of the nanotube wall. (*e*) Zoom of the unit cell and definition of the cell vectors *i* and *j*. The black circles indicate the 2-fold symmetry axes. The β-hairpin backbone of Lanreotide is drawn on the zoom to fit the regions of high (red) and low (blue) electron densities. Note the alternation of low and high electron density areas along *j* and the continuity of these areas along *i*.

stacking of antiparallel peptides (Fig. 4*e*) would be in agreement with both observed repeat distance and aromatic/aliphatic segregation.

Structural Model of Nanotube Wall. The surface S per unit cell is 380 Å^2 and contains two molecules. If we assume that, as for proteins, the Lanreotide density ranges from 1.2 to 1.3, then the volume V of the molecule can be estimated to be 1,400–1,500 Å^3. The thickness t of one fiber estimated by using $t = 2.V/S$ ranges between 7.4 and 8 Å, which is about half the wall thickness of the nanotubes (18 Å). Therefore, two superimposed β-sheet fibers constitute a single filament, which is visualized on the Patterson

Table 1. Nanotube parameters

	a_{hex}, Å	ϕ, Å	d, Å	i (n), Å	j (m), Å	γ, °	S, Å²
Lanreotide	365	244	243	20.7 (13)	20.8 (26)	119.0	377
Derivative	259	166	176	20.2 (11)	21.1 (18)	117.2	380

Supramolecular and molecular parameters of the nanotubes formed by Lanreotide and its derivative in water. Supramolecular parameter: a_{hex} is the hexagonal parameter (Fig. 5d) obtained by SAXS (Fig. 2c), ϕ is the diameter of the nanotubes (Fig. 5c) from SAXS (Fig. 2d), and $d = a_{hex} - \phi/2$ (see text). Molecular parameter calculated from the fiber diffraction X-ray pattern (Fig. 4 and Fig. 6, which is published as supporting information on the PNAS web site, www.pnas.org): i and j are the unit-cell vectors of the bidimensional curved crystal (Fig. 4e), γ is the (i, j) angle, and S is the surface of the unit cell. n and m are the number of filaments whose direction is along i and j, respectively, constituting a nanotube.

function (Fig. 4d). Thus, the amphiphilic nature of the peptide induces the formation of a bilayer (Fig. 5 a and b), in which the confined hydrophobic residues are protected from water by the inner and the outer β-sheet fibers and by the hydrophilic residues.

Four fiber organizations within the filament are in agreement with the alternation of aliphatic and aromatic residues. All of them are constituted by two molecules related by a 2-fold axis. The first two fiber organizations (Fig. 7, which is published as supporting information on the PNAS web site, www.pnas.org) would exhibit a repeat distance equal to four times the hydrogen bond repeat distance of a β-sheet (4.75 Å), i.e., 19.0 Å. These two fiber possibilities are in contradiction with the experimental repeat distances (20.8 Å for Lanreotide and 21.1 Å for its derivative) and, consequently, the fiber solution is among the two other ones. The two remaining fiber solutions (Fig. 5b) would exhibit a repeat distance of $[(4*4.75)^2 + 7^2]^{1/2} = 20.2$ Å, in which the 7 Å represents the length of a shift of one residue along the peptide backbone. Because a filament is constituted by two amphiphilic β-sheet fibers and because a bilayer formed by two identical organizations cannot be spontaneously curved, the organization of the inner and the outer β-sheet fibers has to be different. At the molecular level, the two remaining β-sheet organizations only differ in the nature of the amino acids involved in the intermolecular hydrogen bonds. The stacking of these two different β-sheets, described in Fig. 5b, exhibit 2-fold axes that would meet exactly when aromatic residues interact in a Naph/Tyr/Tyr/Naph sequence. Therefore, we proposed that the filaments are constituted by the association of these two types of fibers.

Considering this structural model of the filaments, the nanotubes would be formed by the self-assembly of 26 identical filaments of Lanreotide (18 identical filaments for the derivative) resulting in the high monodispersity of the nanotube diameter (Fig. 5c and Table 1). Furthermore, fiber diffraction pattern indicates that these filaments coil up around the tube at an angle of 48.5° with respect to the direction of the cylinder axis. Considering this filament orientation, the model gives a hydrogen bond orientation of 29° with respect to the direction of the cylinder axis.

Discussion

Interactions Driving Nanotube Formation. The structure of Lanreotide nanotubes in water reveals the interactions responsible for the self-assembly. Along the three directions of the nanotube wall crystal, the driving forces are the hydrophobic effect generating a bilayer of fibers forming the filament (Fig. 5 a and b), the hydrogen-bond network maintaining the filament structure along the j vector (Fig. 5b), and the hydrophobic effect again stabilizing the lateral packing of 26 filaments along the i vector (Fig. 5c). In addition, the whole structure highlights a systematic
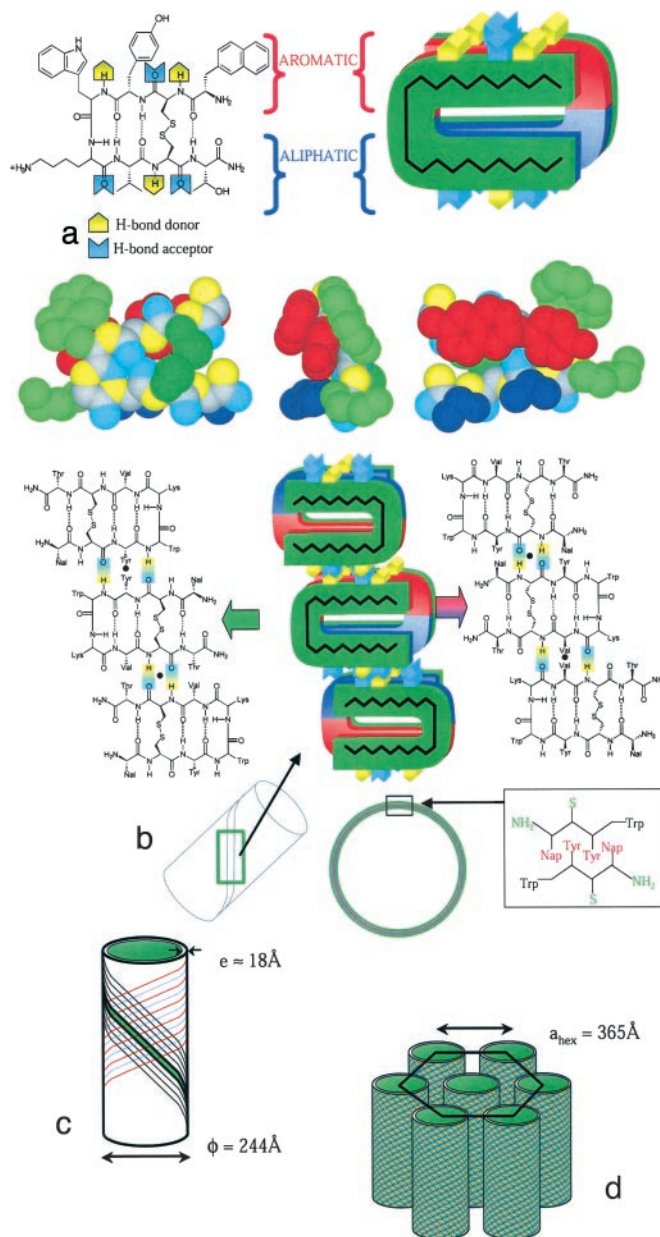

Fig. 5. Schematic view of the different hierarchical levels in the self-assembly of Lanreotide-acetate nanotubes in water. (*a*) (*Left*) The Lanreotide molecule in the β-hairpin planar conformation, which is stabilized by the disulfide bridge, the turn, and intramolecular hydrogen bonds. (*Right*) Interaction between two Lanreotide molecules within the wall (bilayer) of the nanotubes. (*Bottom*) CPK models of a conformation in agreement with experimental data. The segregation of aromatic residues (red) from aliphatic residues (blue) and from hydrophilic region (green) is remarkable. (*b*) The structure of a filament with two different β-sheet fibers superimposed with their C_2 2-fold axes (black circles) meeting together. The segregation between aliphatic/aromatic residues is conserved within the filament organization. (*Inset*) Packing of the aromatic residues within the β-sheet fibers. (*c*) Self-assembly of 26 filaments to form a nanotube. (*d*) Liquid crystalline hexagonal columnar phase formed by the nanotubes.

segregation of aromatic from aliphatic residues. Indeed, filaments exhibit a rigorous and systematic alternation of aromatic and aliphatic regions along the hydrogen bonds direction (*j*) and within the bilayers of fibers (Fig. 5b). Moreover, the Patterson electron density map (Fig. 4e) shows that interactions between filaments lead to the formation of continuous regions of either

aliphatic or aromatic residues along the i vector. This feature essentially results from the constraints exerted by the disulfide bridge and intramolecular interactions on the Lanreotide backbone. Indeed, the resulting β-hairpin conformation enhances the initial segregation present in the peptide sequence.

Implication for β-Sheet Fibrils. E. Gazit (19) recently pointed out the importance of aromatic π-stacking in the self-assembly process leading to amyloid fibrils. This analysis was essentially based on the statistics of aromatic residues occurring in amyloid-related sequences. Similarly, in the two β-strands of the native PrP human prion protein, responsible for the Creutzfeld–Jakob disease (20), three residues among the eight hydrophobic ones are aromatic (tyrosine), suggesting the involvement of aromatic residues in the conformation change of the prion protein. Here we show that aromatic residues are segregated from aliphatic residues in all of the hierarchical levels of the supramolecular organization of Lanreotide nanotubes. Therefore, we propose that the aliphatic/aromatic segregation plays a significant role in the conversion to β-sheet fibrils.

The importance of the peptide charge in the formation of fibrils has been reported (21, 22). Fibrils formation does not occur (*i*) if the peptide charge is vanishing because of precipitation or (*ii*) when the effective charge is too high and inhibits the fiber formation by electrostatic repulsion. In the case of Lanreotide, the effective charge is of +2. A filament in a nanotube is under two electrostatic repulsion forces, one coming from the neighbor filaments in the same nanotube and the other coming from the neighbor nanotubes. The former repulsion tends to increase the size of the nanotube, whereas the latter tends to make it decrease. The electrostatic field generated by the neighbor filaments can be approximated by $\sigma/2\varepsilon$ with σ the surface charge of the wall and ε the dielectric permitivity. For the neighbor nanotubes, the electrostatic field can be estimated in first approximation by $\sigma.\phi/2\varepsilon d$, with ϕ being the nanotube diameter and d being the distance between the considered filament and the center of the neighbor nanotube. The filament would be at mechanical equilibrium when both electric fields are balanced, i.e., when d is $\approx\phi$. This means that the mechanical equilibrium would be reached when the distance between the nanotubes is about their radius (122 Å for Lanreotide and 83 Å for its derivative). The experimental data, for both Lanreotide and derivative, are in agreement with this simple model (Table 1) and suggest that electrostatic forces play a major role in the formation of nanotubes in the hexagonal lattice.

The supramolecular organization of Lanreotide reported here demonstrates that this system is able to investigate the minimal interactions required for generating large self-assembling nanotubes already observed with proteins (23–26) or lipids (27, 28). Furthermore, the potential applications of this type of nanotubes include nanofiltration of biological molecules (29) and templates to fabricate ordered mesoporous materials (1). Currently, a Lanreotide acetate hydrogel of higher concentration than the one studied here is used as a therapeutic in the treatment of acromegaly in the form of a long-acting s.c. implant (Autogel) (12). The exceptional self-assembling properties of Lanreotide acetate in water suggest a correlation between Lanreotide nanotube organization and the controlled release properties of this pharmaceutical product.

1. Dujardin, E. & Mann, S. (2002) *Adv. Mater.* **14,** 775–788.
2. Klug, A. (1983) *Angew. Chem. Int. Ed. Engl.* **22,** 565–636.
3. Nogales, E., Whittaker, M., Milligan, R. A. & Downing, K. H. (1999) *Cell* **96,** 79–88.
4. Kabsch, W., Mannherz, H. G., Suck, D., Pai, E. F. & Holmes, K. C. (1990) *Nature* **347,** 37–44.
5. Holmes, K. C., Popp, D., Gebhard, W. & Kabsch, W. (1990) *Nature* **347,** 44–49.
6. Lehn, J.-M. (1990) *Angew. Chem. Int. Ed. Engl.* **29,** 1304–1319.
7. Krejchi, M. T., Atkins, E. D., Waddon, A. J., Fournier, M. J., Mason, T. L. & Tirrell, D. A. (1994) *Science* **265,** 1427–1432.
8. Gulik-Krzywicki, T., Fouquey, C. & Lehn, J.-M. (1993) *Proc. Natl. Acad. Sci. USA* **90,** 163–167.
9. Bong, D. T., Clark, T. D., Granja, J. R. & Ghadiri, M. R. (2001) *Angew. Chem. Int. Ed.* **40,** 988–1011.
10. Aggeli, A., Boden, N., Keen, J. N., Knowles, P. F., McLeish, T. C. B., Pitkeathly, M. & Radford, S. E. (1997) *Nature* **386,** 259–262.
11. Inouye, H., Fraser, P. E. & Kirschner, D. A. (1993) *Biophys. J.* **64,** 502–519.
12. Cherif-Cheikh, R., Bismuth, F., Torres, M. L., Alloza, R., Bosch, M. T., Montes, M., Fuster, E., Valles, J., Cordero, J. A., Peraire, C., *et al.* (1998) *Proc. Controlled Release Soc.* **25,** 798–799.
13. Narayanan, T., Diat, O. & Boesecke, P. (2001) *Nucl. Instr. Meth. Phys. Res. A* **467,** 1005–1009.
14. Vainshtein, B. K. (1966) in *Diffraction of X-Rays by Chain Molecules* (Elsevier, Amsterdam).
15. De Gennes, P. G. & Prost, J. (1993) *The Physics of Liquid Crystals* (Clarendon, Oxford), 2nd Ed.
16. Levelut, A.-M. (1983) *J. Chim. Phys.* **80,** 149–161.
17. Sugeta, H., Go, A. & Miyazawa, T. (1973) *Bull. Chem. Soc. Jpn.* **46,** 3407–3411.
18. Krimm, S. & Bandekar, J. (1986) *Adv. Protein Chem.* **38,** 181–359.
19. Gazit, E. A. (2002) *FASEB J.* **16,** 77–83.
20. Zahn, R., Liu, A., Lührs, T., Riek, R., von Schroetter, C., López García, F., Billeter, M., Calzolai, L., Wider, G. & Wüthrich, K. (2000) *Proc. Natl. Acad. Sci. USA* **97,** 145–150.
21. Zhang, S., Holmes, T., Lockshin, C. & Rich, A. (1993) *Proc. Natl. Acad. Sci. USA* **90,** 3334–3338.
22. López de la Paz, M., Goldie, K., Zurdo, J., Lacroix, E., Dobson, C. M., Hoenger, A. & Serrano, L. (2002) *Proc. Natl. Acad. Sci. USA* **99,** 16052–16057.
23. Walsby, A. E. (1994) *Microbiol. Rev.* **58,** 94–144.
24. Jiménez, J. L., Guijarro, J. I., Orlova, E., Zurdo, J., Dobson, C. M., Sunde, M. & Saibil, H. R. (1999) *EMBO J.* **18,** 815–821.
25. Van-Raaij, M. J., Mitraki, A., Lavigne, G. & Cusack, S. A. (1999) *Nature* **401,** 935–938.
26. Inouye, H., Bond, J. E., Deverin, S. P., Lim, A., Costello, C. E. & Kirschner, D. A. (2002) *Biophys. J.* **83,** 1716–1727.
27. Lvov, Y. M., Price, R. R., Selinger, J. V., Singh, A., Spector, M. S. & Schnur, J. M. (2000) *Langmuir* **16,** 5932–5935.
28. Hartgerink, J. D., Beniash, E. & Stupp, S. I. (2001) *Science* **294,** 1684–1688.
29. Meller, A., Nivon, L., Brandin, E., Golovchenko, J. & Branton, D. (2000) *Proc. Natl. Acad. Sci. USA* **97,** 1079–1084.